Towards Rational Functionalization of Ionic Liquids for Enhanced Extractive Desulfurization: Computer-aided Solvent Design and Molecular Dynamics Simulation

Jingwen Wang,[a] Zhen Song,[b,c,*] Xinxin Li,[a] Hongye Cheng,[a] Lifang Chen,[a] and Zhiwen Qi[a,*]

[a] *State Key Laboratory of Chemical Engineering, School of Chemical Engineering, East China University of Science and Technology, 130 Meilong Road, 200237, Shanghai, China*

[b] *Process Systems Engineering, Max Planck Institute for Dynamics of Complex Technical Systems, Sandtorstr. 1, D-39106 Magdeburg, Germany*

[c] *Process Systems Engineering, Otto-von-Guericke University Magdeburg, Universitätsplatz 2, D-39106 Magdeburg, Germany*

[*] *Corresponding authors: songz@mpi-magdeburg.mpg.de (Z. S.) ; zwqi@ecust.edu.cn (Z. Q)*

ABSTRACT

Although functionalization is known as a promising way to notably improve the performances of ionic liquids (ILs) in separation processes, studies thereon are mainly experimental trial-and-error based while rational design of functional ILs is scarcely reported. In this work, computer-aided IL design (CAILD) and molecular dynamics (MD) simulation are combined towards rationally functionalizing ILs for the enhanced extractive desulfurization (EDS) of fuel oils. First, the UNIFAC-IL model is extended based on experimental data to specifically cover interaction parameters associated with four functional groups (i.e., hydroxyl, methoxy, vinyl, and cyanomethyl). A mixed-integer nonlinear programming (MINLP) problem is then formulated for the computer-aided design of functional ILs for the EDS task. Finally, MD simulations are performed to study the intermolecular interactions between the top IL candidates and model fuel oil components; by comparing with those for literature-reported ILs, the enhanced EDS performances of the designed functional ILs are well rationalized.

KEYWORDS: functional ionic liquids, extractive desulfurization, UNIFAC-IL, computer-aided ionic liquid design, molecular dynamics

1. INTRODUCTION

Due to the increasing environmental concern on SO_x emissions derived from fuel oil combustion, more and more stringent regulations have been imposed to restrict the sulfur contents in fuel oils.[1,2] As the most industrially used technique, the hydrodesulfurization process suffers from serious disadvantages such as high energy consumption and rigorous reactive conditions.[3,4] In contrast, the extractive desulfurization (EDS) process has shown evident advantages such as mild operating conditions, high selectivity towards aromatic sulfur compounds, thereby attracting considerable attention from both the industry and academia.[5-9]

Of central importance for the EDS process is the selection of a suitable extraction solvent. In the past few years, ionic liquids (ILs) have been extensively explored as alternatives to organic solvents (e.g., *N*,*N*-dimethylformamide, *N*-methyl-2-pyrrolidinone) for this process due to their unique properties, such as negligible volatility, high chemical/thermal stability, and wide liquid range.[10] More interestingly, their thermodynamic and physico-chemical properties can be readily tuned by the judicious selection of cation, anion, and substituent groups, making them "designer solvents".[11-13]

So far, most IL-based EDS studies have mainly focused on the experimental test of different ILs, which is costly, time-consuming, and even impossible for extensive solvent selection considering the great quantity of possible cation-anion combinations.[14-16] In this context, COSMO-based activity coefficient models (i.e., COSMO-RS and COSMO-SAC) have been applied for the theoretical screening of ILs for the EDS as well as other separation processes.[17-25] However, such results are basically qualitative as these predictive models merely rely on quantum-chemically derived molecular descriptors. In recent years, the UNIFAC (UNIversal quasichemical Functional-group Activity Coefficients) model is gradually extended to cover {IL + conventional solute} systems for two main reasons as follows. (1) The quantitative prediction accuracy can be secured as the binary group

interaction parameters are fit from experimental data. (2) The group contribution (GC) character makes it well suited to be integrated into the computer-aided molecular design (CAMD) framework for designing IL solvents.[26-29] Taking account of these merits, our group recently reported a systematic CAILD work on the EDS task based on the UNIFAC-IL model extension. The designed ILs were found to have much better process performance than the benchmark organic solvent sulfolane.[30]

Despite the progress made, the above CAILD work as well as similar studies on other separations simply considered the variation of cation, anion, and alkyl side chain length. In other words, such CAILD is still limited to the space of conventional ILs.[31,32] However, many studies have found that functionalizing ILs by introducing functional groups (e.g., ether, amino, and hydroxyl) is a promising way to significantly enhance the solvent performances of ILs.[33-37] For instance, Zeng et al. developed tertiary amino-, ether-, and nitrile-functionalized ILs ([NEt_2C_2Py][SCN], [C_4OPy][SCN], and [C_4CNPy][SCN]) for SO_2 absorption, which are all experimentally proved to exhibit much better absorption capacity and SO_2/CO_2 selectivity than the benchmark conventional IL [C_4Py][SCN].[38] Kianpour and his coworkers reported that the one-stage dibenzothiophene removal efficiencies of acetate-functionalized [TBCMP][Br] and ether-functionalized [TBHEP][Br] are 2 – 4 times higher in comparison with the benchmark [TBEP][Br].[33,39] These experimental findings suggest that functionalization of ILs is highly worth to be studied for the development of more efficient separation processes. However, as the synthesis and purification of functional ILs could be more complex and demanding than conventional ILs, one can of course not rely on experimental method to explore the various possibilities for IL functionalization at the early stage. In this sense, it is strongly desirable for the further development of CAILD to cover various functional ILs. Besides, knowing that CAILD output only the information of potential IL structures from the given set of molecular building blocks, it is also of high interest to

study the microscopic behaviors of the designed ILs in the mixture to be separated. This could for one thing act as valuable post-design analysis of the obtained ILs before final experimental verification and for another offer useful insights to reversely modulate the CAILD.[40-44]

Taking account of the aforementioned aspects, this contribution combines CAILD and molecular dynamics (MD) simulation to rationally identify functional ILs as solvents for EDS. To begin with, the UNIFAC-IL model is extended to cover interaction parameters related to four functional groups for the purpose of CAILD. Based on the obtained UNIFAC-IL model and available GC models for IL physical properties, a mixed-integer nonlinear programming (MINLP) problem is formulated for the design of functional ILs. Finally, MD simulations are carried out for the {IL + model fuel oil} systems, where the microscopic behaviors of the designed functional ILs and benchmark conventional ILs are compared.

2. UNIFAC-IL MODEL EXTENSION

The original UNIFAC model was first proposed by Fredenslund et al. in 1975[45] and was recently proved as a powerful tool to predict thermodynamic properties of IL-involved systems.[26-30,46] For the functional IL design task, the UNIFAC-IL model is further extended in this work to cover the missing interaction parameters associated with four functional groups namely hydroxyl (OH), methoxy (OCH_3), vinyl (CH_2=CH), and cyanomethyl (CH_2CN).

Like in other GC methods, IL molecules have to be decomposed into separate groups for UNIFAC-IL extension. In this work, ILs are divided into several groups including cation skeletons, anions, and substituents.[28,30] For example, [C_4MIm][BF_4] is composed of one CH_3, three CH_2, one MIm^+ (1-sub-3-methylimidazolium) together with one BF_4^- group. This group decomposition method is constant with that in most GC models for physical properties of ILs and could also enlarge the space and flexibility of CAILD.[47-49]

The original UNIFAC model calculates activity coefficient (γ) in two parts:

$$\ln \gamma = \ln \gamma_i^C + \ln \gamma_i^R \quad (1)$$

where $\ln \gamma_i^C$ represents the combinatorial contribution and accounts for the size and shape of groups; $\ln \gamma_i^R$ refers to the residual contribution, essentially due to the energetic interactions between groups. The calculation of $\ln \gamma_i^C$ requires the relative van der Waals group volumes (R_k) and relative van der Waals group surfaces (Q_k), which can be taken directly from literatures for already existing groups and determined for new IL groups as:

$$R_k = \frac{V_k \times N_A}{15.17} \quad (2)$$

$$Q_k = \frac{A_k \times N_A}{2.5*10^9} \quad (3)$$

where V_k (group volume) and A_k (group area) can be obtained by molar volume and surface area correlations[49] or quantum chemical calculations.[29,50-51] N_A refers to the Avogardro's number (6.023×10^{23} mol^{-1}). Q_k and R_k of the involved cation skeletons, anions, and substituent groups in this work are listed in Table S1 (Supporting Information).

The residual part can be expressed as the function of binary interaction parameters (i.e., a_{nm} and a_{mn}) associated with the involved main groups.[45] To determine the missing interaction parameters for pairwise functional groups and IL (cation skeleton, anion) groups, available experimental infinite dilution activity coefficients (γ^∞) of relevant solutes in ILs are collected from literature (see the detailed data and references in Table S2, Supporting Information). As shown, the involved solutes cover alcohols (ethanol, 1-propanol, 1-butanol), ethers (methyl tert-butyl ether, tert-butyl ethyl ether, tert-amyl methyl ether, ethyl ether), olefins (1-hexene, 1-heptene, 1-octene), and acetonitrile; the involved 68 ILs are of different cations and anion types, which also include ILs containing the four functional groups, such as $[CH_3OC_2MPyr][FAP]$ and $[CH_2{=}CHC_1MIm][NTf_2]$ (see Table S2, Supporting Information). One should note that the interaction parameters between cation skeleton and anion are

assumed to be zero because of the strong interaction and weak dissociation of ion pairs, and the ones for the existing UNIFAC functional groups are directly withdrawn from previous studies.[30] All the 2870 data in Table S2 are taken as the model regression database to cover as many as possible binary interaction parameters. Totally, 154 pairs of missing functional group-IL group interaction parameters are obtained by minimizing:

$$OF = \frac{100\%}{N_d}\sum_{1}^{N_d}\left|\frac{\gamma_i^{\infty,\exp}-\gamma_i^{\infty,cal}}{\gamma_i^{\infty,\exp}}\right| \quad (4)$$

where $\gamma_i^{\infty,\exp}$, $\gamma_i^{\infty,cal}$ represent the experimental and UNIFAC-IL calculated γ^{∞}, and N_d is the total number of data points (here, N_d = 2870). The optimization problem is solved by the "fmincon" solver in Matlab, where several sets of initial values within different ranges (-1000 to 1000) are randomly generated and tested. For each initialization, the optimization run was terminated when the relative deviation of a_{nm} and a_{mn} between iterations was less than 0.001. The results shows that the objective function values obtained from some of the initial guesses are very close; nevertheless, the best solution having the smallest objective function value is finally presented (see Table 1).

To preliminarily evaluate the reliability of the obtained model, the $\gamma_i^{\infty,\exp}$ and $\gamma_i^{\infty,cal}$ in the model regression database are compared. As depicted in the parity plot Figure 1a, the predicted data for the four types of solutes fall almost evenly in a small range close to the diagonal. To be specific, the average relative deviations (*ARD*s) in the four cases are 16.37% (1002 data points for alcohols), 25.52% (750 data points for ethers), 27.52% (892 data points for olefins), 6.26% (226 data points for acetonitrile), respectively, which are all in a very low level.[31,32] Moreover, from the distribution of data points within different ranges of *ARD*s in Figure 1b, the majority of the overall data (72.6%) present *ARD*s lower than 20% while for only 7.7% of them the *ARDs* go beyond 40%. For the overall 2870 points, the average *ARD* is 21.4%, suggesting the good γ^{∞} prediction reiability of the obtained UNIFAC-IL model.

To further estimate the reliability of the UNIFAC-IL model, the liquid-liquid equilibria (LLE) prediction of IL-containing systems is also tested. For this purpose, the LLE of 35 functional-IL-involved ternary systems (10 {IL + aromatic + aromatic/cycloalkane/alkane}, 5 {IL + S-compound + aromatic/cycloalkane/alkane}, 11 {IL + alkene + alkane} and 9 {IL + alcohol + alkane/alkene/ester}) and 66 binary systems of {IL + thiophene/aromatic/cycloalkane/alkane} are calculated and compared to the experimental data (see Tables S3 and S4 in Supporting Information for the detailed data and references) by the root mean square deviation (*RMSD*):

$$RMSD = \left\{ \sum_{i} \sum_{p} \sum_{t} \left(x_{ipt}^{\exp} - x_{ipt}^{cal} \right)^2 \Big/ 6N_t \right\}^{1/2} \qquad (5)$$

where the subscripts *i*, *p*, and *t* represent the component, the phase, and the tie-line, respectively; *x* is the mole fraction and N_t stands for the total number of tie-lines.

For these different ternary LLE, the *RMSD*s are 0.0577, 0.0499, 0.0176, and 0.0654, respectively, with an average *RMSD* of 0.0507 for the overall 35 systems. For a clear illustration, Figure 2 illustrates the comparison of experimental and predicted LLE of {[OHC_3Py][$N(CN)_2$] + cyclohexene + cyclohexane}, {[COC_2mPip][NTf_2] + *n*-heptane + methanol}, {[CH_2=CHC_1Mor][NTf_2] + benzene + *n*-hexane}, and {[C_3CNPy][$N(CN)_2$] + styrene + ethylbenzene}, which are the representatives based on the OH-, OCH_3-, CH_2=CH-, and CH_2CN-functionalized ILs, respectively. As seen, the predicted LLE compositions for these four systems only differ slightly from the experimental ones. Besides, by comparing the experimental and calculated binary LLE, it is found that the effect of temperature on the *T*-*x* compositions is in most cases qualitatively correct but not well captured from quantitative point of view. Such a deficiency is understandable as the model following the original UNIFAC form only includes two temperature-independent interaction parameters between two main groups. Nevertheless, the structural effects of ILs and solutes on the binary LLE are

correctly predicted, which still leads to an acceptable average *RMSD*s of 0.0962 for the overall 613 *T*-*x* compositions. Considering that the model are regressed from γ^{∞} data only and 34 of the involved ternary and binary systems are based on ILs not included in the model regression database, the LLE database are highly qualified as the external validation set. Therefore, based on the LLE validation results, it can be inferred that the extended UNIFAC-IL model can be employed as a reliable tool for predicting thermodynamic properties in the functional ILs design.

3. COMPUTER-AIDED IONIC LIQUID DESIGN

CAILD has been increasingly used to reverse IL structures that best meet the desired target properties in various applications.[22,25,29,30,52-54] In this section, a CAILD framework is employed to design functional ILs for the EDS process, which consists of four steps.

Step 1: Specify the target mixture to be separated. In this case, the fuel oil is modeled by a four-component mixture of {*n*-octane (1) + toluene (2) + cyclohexane (3) + thiophene (4)} with a mass fraction of [0.70, 0.15, 0.15, 100 ppm], and the mass ratio of IL to the model fuel oil mixture in EDS is fixed to 1:1.[30]

Step 2: Determine the basis set of IL building blocks. To increase the IL design space, all the cation and anion groups with available parameters in the employed thermodynamic and physical property models are included in the group basis set for CAILD. Moreover, apart from the conventional groups used in the very recent work,[30] the four functional groups (OH, OCH_3, CH_2=CH, and CH_2CN) are added in this design task. The substituents, cation skeletons, and anions in the final basis set can be seen in lines 1 – 7, 8 – 20, and 21 – 27 of Table S1 (Supporting Information).

Step 3: Formulate the mixed integer nonlinear program (MINLP) as follows:

$$\textbf{\textit{Objective function}} \qquad \max\left\{PI = \beta \times S\right\} \tag{6}$$

s.t. *IL structural constraints*

Thermodynamic property constraints

Physical property constraints

The overall performance index (*PI*) is defined as the product of mass-based distribution coefficient (β) and selectivity (*S*), which can be calculated based on the UNIFAC-IL model by Eqs. (7) – (8):

$$\beta = \frac{m_4^E}{m_4^R} \tag{7}$$

$$S = \frac{m_4^E}{m_4^R} \Big/ \frac{(m_1^E + m_2^E + m_3^E)}{(m_1^R + m_2^R + m_3^R)} \tag{8}$$

where the superscripts *E* and *R* stand for the extraction and raffinate phase; m_1, m_2, m_3, and m_4 represent the mass fractions of *n*-octane, toluene, cyclohexane, and thiophene in the calculated LLE of the EDS system, respectively.

The structural constraints include structural feasibility rules (Eqs. (9) – (11)) and complexity rules (Eqs. (12) – (14)):

$$\sum_{j \in Ca} c_j = 1 \tag{9}$$

$$\sum_{j \in An} c_j = 1 \tag{10}$$

$$\sum_{j \in Ca,Sub} (2 - v_j) \times c_j - 2 = 0 \tag{11}$$

$$1 \le \sum_{k \in Sub} c_k \le 10 \tag{12}$$

$$\sum_{k \in CH_3, CH_2} c_k \ge 1 \tag{13}$$

$$\sum_{k \in Sub^*} c_k = 1 \tag{14}$$

where *Ca* and *An* stand for the subsets of cation skeletons and anions in the group basis set,

respectively; v_j denotes the valence of group j; *Sub* refers to the subset of substituent groups on the cation side chain in the group basis set while *Sub** represents the subset of functional substituent groups (i.e., substituent groups except for CH_3 and CH_2). Eqs. (9) and (10) guarantee only one pair of cation skeleton and anion will be selected in each generated IL. Eq. (11), the octet rule, ensures no free bonds in cations; Eq. (12) limits the number of substitute groups in ILs within the bound 1 – 10; Eq. (13) restricts at least one CH_3/CH_2 group on the substitute and Eq. (14) imposes only one functional substituent group.

In addition, to find out ILs possessing satisfactory β and S, the thermodynamic property constraints are considered.

$$\beta > \beta_{\text{sulfolane}} \tag{15}$$

$$S > S_{\text{sulfolane}} \tag{16}$$

As seen, sulfolane, one of the most promising conventional solvents for the EDS process, is introduced as the benchmark for the thermodynamic properties of IL solvents.[19,30]

Regarding the physical property constraints, the melting point (T_{m}) and viscosity (η) of ILs are considered to ensure that the designed ILs are liquid at room temperature ($T_{\text{m}} \leq 298.15$ K) and have relatively low viscosity ($\eta \leq 50$ *cP*). These two physical properties are estimated by two GC models developed by Lazzús et al.[47,48]

Step 4: Solve the MINLP problem. In this work, the generate-and-test approach is utilized.[31,32] To be specific, the MINLP program is decomposed into an ordered set of subproblems and each of them requires the solution of only one corresponding constraint. The solutions that pass through all the subproblems are retained as the potential IL solvents. In subproblem 1, an initial number of 6893 ILs candidates are enumerated following the structural constraints. Then, by the thermodynamic property constraints in subproblem 2, 701 IL candidates are retained possessing both higher β and S than sulfolane. Finally, 127 of them

further satisfy the constraints on the T_m and η.

The top five IL candidates having the highest *PI* are listed in Table 2 together with the predicted properties, and their structures are depicted in Figure 3. As seen, they are all combinations of a $[C(CN)_3]^-$ anion and a vinyl-functionalized pyridinium cation. Interestingly, these functional IL candidates have identical anion and cation skeleton as the optimal conventional ILs that can be designed on the same group basis set without functional groups.[30] However, as compared in Figure 4, the β of the functional ILs identified here (1.79 – 1.98) are notably higher than that of the conventional ones (0.95 – 1.21) while their *S* almost remain at the same level. Consequently, the *PI* of the functional ILs is nearly 1.5 times higher, demonstrating an enhanced separation performance of them from the thermodynamic point of view. In previous EDS literature, pyridinium based ILs have not been studied as extensively as imidazolium-based ones which has the potential advantages such as relatively simple preparation and easy structure tunability. However, the CAILD results suggest that pyridinium based ILs are worthy of more study due to their higher thermodynamic properties (mainly a higher β due to stronger van der Waals interactions with S-compound)[18,20] and comparative physical properties.

4. MOLECULAR DYNAMICS SIMULATION

MD simulations or quantum chemical calculations can be employed to study the microscopic behaviors of ILs in the EDS system and provide insights into the enhancement mechanisms of functional ILs, thereby acting as an important post-design validation.[35,55] As the top five candidates only differ slightly from each other in the alkyl chain length, the first one $[CH_2{=}CHC_1MPy][C(CN)_3]$ is taken as the representative. Moreover, for a clear comparison of the effect of functionalization, the first conventional IL $[C_2MPy][C(CN)_3]$ reported previously[30] is taken as a benchmark.

In this section, MD simulations are performed in an isothermal-isobaric ensemble (NPT)

using the GROMACS code. Figure 5 shows the optimized structures of the involved components in the simulated EDS systems based on B3LYP/6-31++G** theoretical level together with the atom labels. Then the partial atomic charges are derived from above geometric optimizations by the RESP method using the Restrained ESP Fit package implemented in the AMBER 4.1 program. The relevant force field parameters for these components are obtained from the Amber force field, which is commonly used in the IL-involved MD simulations.[43,56-58] The cutoff distance is set to be 1.5 nm for Coulomb and Lenard-Jones (LJ) short-range interactions, beyond which particle mesh Ewald (PME) method is used to compute the long-range electrostatic interactions with 0.16 nm grid spacing and fourth-order interpolation. The V-rescale thermostat method is used for maintaining 298.15 K for the simulated systems while the pressure is scaled with Parrinello-Rahman barostat method at 1 bar.

The fixed global composition of the EDS system in the CAILD corresponds to a molecular number ratio of 5100: 1350: 1485: 1: 3700/3900 for *n*-octane: toluene: cyclohexane: thiophene: functional/conventional IL. However, considering the intensive computation load required for such a large quantity of molecules, the mass fraction of thiophene is enlarged to 5000 ppm in the MD simulations. Correspondingly, 306 *n*-octane, 81 toluene, 89 cyclohexane, 6 thiophene, 222/234 pairs of ions are included in the {functional/conventional IL + model fuel oil} systems. The simulations are performed starting from a low-density $8 \times 8 \times 8$ nm^3 initial box being equilibrated for 4 ns and the last 2 ns is used to collect data for radial distribution function (RDF), spatial distribution function (SDF) and energy analyses. Visual molecular dynamics (VMD 1.9.3) package is applied to extract visual models of the systems.

First, the intermolecular interactions between IL and the sulfur-compound thiophene are analyzed from SDFs, site-site RDFs, and interaction energies. From the SDF results in Figure 6, the anion $[C(CN)_3]^-$ and cation skeleton MPy^+ of these two ILs distribute around

thiophene almost in the same pattern. Specifically, the anion mainly surrounds the H atoms of thiophene, indicating the interactions between the N atoms of $[C(CN)_3]^-$ and the H atoms of thiophene; meanwhile, the pyridinium ring of cation is mainly located parallel to the plane of thiophene, which suggests the formation of π-π interactions.[41,43] The major differences in the SDFs for the {functional IL + model fuel oil} and {conventional IL+ model fuel oil} systems lie in the distributions of the cation substituent groups surrounding thiophene. As seen, the vinyl-functionalized substituent group (–C–C=C) of the functional IL is much more densely distributed around thiophene in comparison to the $–C_2H_5$ group of the conventional IL, implying the stronger interactions between the functional substituent group and thiophene. The stronger interactions between –C–C=C group and thiophene over those between $–C_2H_5$ group and thiophene are also revealed from the corresponding RDF analyses. From Figure 7, the first maximum peak for the RDF between thiophene and methylene in the functional –C–C=C group (solid line) is located near 3.6855 Å for the S1···C8 pair (see atom labels in Figure 5), which is much shorter than that between thiophene and methylene in the conventional $–C_2H_5$ group (3.9285 Å, dash line). Moreover, the RDFs of S1···C18 and S1···C20 for the thiophene – vinyl group pair (solid line) have intense peaks at about 3.7 Å, which are also shorter than the interaction distance between thiophene and methyl in the $–C_2H_5$ group (3.8475 Å for the S1···C18 pair, dash line). The consistent RDF and SDF results are further evidenced by the interaction energy analyses for the {functional/conventional IL + model fuel oil} systems. As seen from Table S5 (Supporting Information), the anion – thiophene interactions are almost the same (-266.60 kJ/mol vs. -267.20 kJ/mol) in the systems based on different ILs whereas thiophene has a notably higher interaction with the vinyl-functionalized cation in comparison to the conventional cation (-150.26 kJ/mol vs. -145.55 kJ/mol), accounting for the positive effect of the introduced –C–C=C group. All these findings demonstrate that –C–C=C group interacts more strongly with thiophene than $–C_2H_5$

group does, thereby the higher β of functional IL than that of the conventional one can be well understood.

Moving beyond the IL – thiophene interaction analyses, those between IL and the non-sulfur fuel component (*n*-octane, toluene, cyclohexane) are further investigated. Figure 8 compares the corresponding RDFs associated with the substituent group in these cases. As seen in Figure 8a, the RDFs of C1···C8, C1···C18 and C1···C20 for the interactions between *n*-octane (C1 atom) and –C–C=C (solid line) locate at about 4.5 Å, which are almost the same location as those between *n*-octane and $–C_2H_5$ group pair (dash line). From Figures 8b and 8c, the interaction distances of –C–C=C group – toluene (3.8475 – 4.0905 Å) and –C–C=C group – cyclohexane (4.0095 – 4.8195 Å) pairs (solid line) are both shorter than those in the case of $–C_2H_5$ group (dash line), which are 3.9285 – 4.1715 Å, 4.1715 – 4.9815 Å, respectively. Comparing with the substituent – thiophene interactions shown in Figure 7 (3.6855 – 3.7655 Å for –C–C=C group – thiophene, 3.8475 – 3.9285 Å for $–C_2H_5$ group – thiophene), the notably longer RDF locations between substituent and the non-sulfur fuel component (*n*-octane, toluene, cyclohexane) in these two systems demonstrate that both the functional IL and conventional IL interacts preferentially with thiophene over these non-sulfur components, which agrees well with their high EDS selectivity (from 14.10 to 19.57, Figure 4b). Besides, as the interactions between the –C–C=C group and thiophene/toluene/cyclohsexane enhance to a similar extent in comparison to the $–C_2H_5$ case, the *S* of the vinyl-functionalized IL are almost at the same level as conventional $[C_2MPy][CCN)_3]$.

From above, the promising EDS performance of the ILs identified by CAILD is well demonstrated from the microscopic point of view. Moreover, through the comparison of MD results, the higher β and *S* of the designed functional IL than the benchmark conventional IL are also elucidated.

5. CONCLUSION

This work particularly combines the CAILD and MD simulation towards the rational identification of functional ILs for the EDS of fuel oils. The UNIFAC-IL model is extended to cover 154 missing interaction parameters related to four functional groups (OH, OCH_3, CH_2=CH, and CH_2CN) by experimental data. Following this, a MINLP problem is formulated and solved for the computer-aided design of functional ILs. The top five candidates are all combinations of a $[C(CN)_3]^-$ anion and a vinyl-functionalized pyridinium cation. Comparing with the conventional benchmark IL with the same cation skeleton and anion, the designed functional ILs have a notably improved separation performance index (*PI*) due to a much higher β and almost constant *S*. The enhanced EDS performance of the designed ILs is well interpreted and understood by the MD simulations of {IL + model fuel oil} systems.

These encouraging results demonstrate that vinyl functionalization is a promising way to improve the EDS performance of ILs. In future work, the UNIFAC-IL model could be further extended to cover more potential groups to enlarge the space for functional IL design. Moreover, other theoretical approaches such as quantum chemical calculations could also be utilized in the post-designed validation to unveil the enhancement mechanisms of ILs identified by CAILD. Of course, the experimental synthesis and validation of the designed functional ILs should be pursued to finally identify practically promising EDS solvents. The proposed framework could be easily extended to support the rational functionalization of ILs for other separation processes.

ASSOCIATED CONTENT

Supporting Information

Table S1: R_k and Q_k for groups involved in the extended UNIFAC-IL model; Table S2: Comparison of experimental and UNIFAC-IL calculated γ^{∞} for different solutes in ILs; Table S3: Detailed ternary LLE database used for UNIFAC-IL validation; Table S4. Detailed binary

LLE database used for UNIFAC-IL validation; Table S5: Interaction energies for cation – thiophene and anion – thiophene in the {functional/conventional IL + model fuel oil} systems. The Supporting information associated with this article can be found online at ****.

ACKNOWLEDGEMENT

The financial support from National Natural Science Foundation of China (21576081, 21776074 and 2181101120) is greatly acknowledged.

REFERENCES

(1) Jiang, W.; Zhu, W.; Chang, Y.; Chao, Y.; Yin, S.; Liu, H.; Zhu, F.; Li, H. Ionic liquid extraction and catalytic oxidative desulfurization of fuels using dialkylpiperidinium tetrachloroferrates catalysts. *Chem. Eng. J.* **2014,** *250*, 48-54.

(2) Liao, J. J.; Wang, Y. S.; Chang, L. P.; Bao, W. R. A process for desulfurization of coking benzene by a two-step method with reuse of sorbent/thiophene and its key procedures. *Green Chem.* **2015,** *17*, 3164-3175.

(3) Carrado, K. A.; Kim, J. H.; Song, C. S.; Castagnola, N.; Marshall, C. L.; Schwartz, M. M. HDS and deep HDS activity of CoMoS-mesostructured clay catalysts. *Catal. Today* **2006,** *116*, 478-484.

(4) Bosmann, A.; Datsevich, L.; Jess, A.; Lauter, A.; Schmitz, C.; Wasserscheid, P. Deep desulfurization of diesel fuel by extraction with ionic liquids. *Chem. Commun.* **2001,** *23*, 2494-2495.

(5) Kianpour, E.; Azizian, S. Polyethylene glycol as a green solvent for effective extractive desulfurization of liquid fuel at ambient conditions. *Fuel* **2014,** *137*, 36-40.

(6) Wang, J. L.; Zhao, R. J.; Han, B. X.; Tang, N.; Li, K. X. Extractive and oxidative desulfurization of model oil in polyethylene glycol. *Rsc Adv.* **2016,** *6*, 35071-35075.

(7) Zhang, S. G.; Zhang, Q. L.; Zhang, Z. C. Extractive desulfurization and denitrogenation of fuels using ionic liquids. *Ind. Eng. Chem. Res.* **2004,** *43*, 614-622.

(8) Wilfred, C.D.; Kiat, C.F.; Man, Z.; Bustam, M. A.; Mutalib, M. I. M.; Phak, C. Z. Extraction of dibenzothiophene from dodecane using ionic liquids. *Fuel Process Technol.* **2012,** *93*, 85-89.

(9) Gao, S. R.; Chen, X. C.; Xi, X. T.; Abro, M.; Afzal, W.; Abro, R.; Yu, G. R. Coupled Oxidation-Extraction Desulfurization: A Novel Evaluation for Diesel Fuel. *ACS Sustainable Chem. Eng.* **2019,** *7*, 5660-5668.

(10) Quijada-Maldonado, E.; Meindersma, G. W.; de Haan, A. B. Pilot plant study on the extractive distillation of toluene-methylcyclohexane mixtures using NMP and the ionic liquid [hmim][TCB] as solvents. *Sep. Purif. Technol.* **2016,** *166*, 196-204.

(11) Abro, R.; Abdeltawab, A. A.; Al-Deyab, S. S.; Yu, G. R.; Qazi, A. B.; Gao, S. R.; Chen, X. C. A review of extractive desulfurization of fuel oils using ionic liquids. *Rsc Adv.* **2014,** *4*, 35302-35317.

(12) Dong, K.; Liu, X. M.; Dong, H. F.; Zhang, X. P.; Zhang, S. J. Multiscale Studies on Ionic Liquids. *Chem. Rev.* **2017,** *117*, 6636-6695.

(13) Ventura, S. P. M.; Silva, F. A. E.; Quental, M. V.; Mondal, D.; Freire, M. G.; Coutinho, J. A. P. Ionic-Liquid-Mediated Extraction and Separation Processes for Bioactive Compounds: Past, Present, and Future Trends. *Chem. Rev.* **2017,** *117*, 6984-7052.

(14) Ahmed, O. U.; Mjalli, F. S.; Talal, A. W.; Al-Wahaibi, Y.; Nashef, I. M. Extractive

Desulfurization of Liquid Fuel using Modified Pyrollidinium and Phosphonium Based Ionic Liquid Solvents. *J. Solution Chem.* **2018,** *47*, 468-483.

(15) Alonso, L.; Arce, A.; Francisco, M.; Rodriguez, O.; Soto, A. Gasoline desulfurization using extraction with [C_8mim][BF_4] ionic liquid. *AlChE J.* **2007,** *53*, 3108-3115.

(16) Rodriguez-Cabo, B.; Francisco, M.; Soto, A.; Arce, A. Hexyl dimethylpyridinium ionic liquids for desulfurization of fuels. Effect of the position of the alkyl side chains. *Fluid Phase Equilib*. **2012,** *314*, 107-112.

(17) Paduszynski, K.; Domanska, U., COSMO-RS screening for ionic liquid to be applied in extraction of 2-phenylethanol from aqueous solutions. *J. Mol. Liq.* **2018,** *271*, 305-312.

(18) Ferreira, A. R.; Freire, M. G.; Ribeiro, J. C.; Lopes, F. M.; Crespo, J. G.; Coutinho, J. A. P. Ionic liquids for thiols desulfurization: Experimental liquid-liquid equilibrium and COSMO-RS description. *Fuel* **2014,** *128*, 314-329.

(19) Song, Z.; Zhou, T.; Qi, Z.; Sundmacher, K. Systematic Method for Screening Ionic Liquids as Extraction Solvents Exemplified by an Extractive Desulfurization Process. *ACS Sustainable Chem. Eng.* **2017,** *5*, 3382-3389.

(20) Song, Z.; Zhou, T.; Zhang, J. A.; Cheng, H. Y.; Chen, L. F.; Qi, Z. W. Screening of ionic liquids for solvent-sensitive extraction -with deep desulfurization as an example. *Chem. Eng. Sci.* **2015,** *129*, 69-77.

(21) Wilfred, C. D.; Man, Z.; Chan, Z. P. Predicting methods for sulfur removal from model oils using COSMO-RS and partition coefficient. *Chem. Eng. Sci.* **2013,** *102*, 373-377.

(22) Zhang, J. A.; Qin, L.; Peng, D. L.; Zhou, T.; Cheng, H. Y.; Chen, L. F.; Qi, Z. W. COSMO-descriptor based computer-aided ionic liquid design for separation processes Part II:

Task-specific design for extraction processes. *Chem. Eng. Sci.* **2017,** *162*, 364-374.

(23) Gonzalez-Miquel, M.; Palomar, J.; Omar, S.; Rodriguez, F. CO_2/N_2 Selectivity Prediction in Supported Ionic Liquid Membranes (SILMs) by COSMO-RS. *Ind. Eng. Chem. Res.* **2011,** *50*, 5739-5748.

(24) Palomar, J.; Torrecilla, J. S.; Ferro, V. R.; Rodriguez, F. Development of an a priori ionic liquid design tool. 1. Integration of a novel COSMO-RS molecular descriptor on neural networks. *Ind. Eng. Chem. Res.* **2008,** *47*, 4523-4532.

(25) Wang, J.; Song, Z.; Cheng, H.; Chen, L.; Deng, L.; Qi, Z. Computer-Aided Design of Ionic Liquids as Absorbent for Gas Separation Exemplified by CO_2 Capture Cases. *ACS Sustainable Chem. Eng.* **2018,** *6*, 12025-12035.

(26) Hector, T.; Gmehling, J. Present status of the modified UNIFAC model for the prediction of phase equilibria and excess enthalpies for systems with ionic liquids. *Fluid Phase Equilib*. **2014,** *371*, 82-92.

(27) Lei, Z. G.; Dai, C. N.; Liu, X.; Xiao, L.; Chen, B. H. Extension of the UNIFAC Model for Ionic Liquids. *Ind. Eng. Chem. Res.* **2012,** *51*, 12135-12144.

(28) Lei, Z. G.; Zhang, J. G.; Li, Q. S.; Chen, B. H. UNIFAC Model for Ionic Liquids. *Ind. Eng. Chem. Res.* **2009,** *48*, 2697-2704.

(29) Roughton, B. C.; Christian, B.; White, J.; Camarda, K. V.; Gani, R. Simultaneous design of ionic liquid entrainers and energy efficient azeotropic separation processes. *Compu. Chem. Eng.* **2012,** *42*, 248-262.

(30) Song, Z.; Zhang, C.; Qi, Z.; Zhou, T.; Sundmacher, K. Computer-aided design of ionic liquids as solvents for extractive desulfurization. *AlChE J.* **2018,** *64*, 1013-1025.

(31) Song, Z.; Li, X.; Chao, H.; Mo, F.; Zhou, T.; Cheng, H.; Chen, L.; Qi, Z. Computer-aided ionic liquid design for alkane/cycloalkane extractive distillation process. *Green Energy Environ.* **2019,** *4*, 154-165.

(32) Chao, H.; Song, Z.; Cheng, H. Y.; Chen, L. F.; Qi, Z. W. Computer-aided design and process evaluation of ionic liquids for n-hexane-methylcyclopentane extractive distillation. *Sep. Purif. Technol.* **2018,** *196*, 157-165.

(33) Kianpour, E.; Azizian, S.; Yarie, M.; Zolfigol, M. A.; Bayat, M. A task-specific phosphonium ionic liquid as an efficient extractant for green desulfurization of liquid fuel: An experimental and computational study. *Chem. Eng. J.* **2016,** *295*, 500-508.

(34) Moghadam, F. R.; Azizian, S.; Bayat, M.; Yarie, M.; Kianpour, E.; Zolfigol, M. A. Extractive desulfurization of liquid fuel by using a green, neutral and task specific phosphonium ionic liquid with glyceryl moiety: A joint experimental and computational study. *Fuel* **2017,** *208*, 214-222.

(35) Ren, Z. Q.; Zhou, Z. Y.; Li, M. X.; Zhang, F.; Wei, L.; Liu, W. D. Deep Desulfurization of Fuels Using Imidazole Anion-Based Ionic Liquids. *ACS Sustainable Chem. Eng.* **2019,** *7*, 1890-1900.

(36) Zhao, H.; Baker, G. A.; Wagle, D. V.; Ravula, S.; Zhang, Q. Tuning Task-Specific Ionic Liquids for the Extractive Desulfurization of Liquid Fuel. *ACS Sustainable Chem. Eng.* **2016,** *4*, 4771-4780.

(37) Paduszynski, K.; Krolikowski, M.; Zawadzki, M.; Orzel, P. Computer-Aided Molecular Design of New Task-Specific Ionic Liquids for Extractive Desulfurization of Gasoline. *ACS Sustainable Chem. Eng.* **2017,** *5*, 9032-9042.

(38) Zeng, S. J.; He, H. Y.; Gao, H. S.; Zhang, X. P.; Wang, J.; Huang, Y.; Zhang, S. J. Improving SO_2 capture by tuning functional groups on the cation of pyridinium- based ionic liquids. *Rsc Adv.* **2015,** *5*, 2470-2478.

(39) Moghadam, F. R.; Azizian, S.; Kianpour, E.; Yarie, M.; Bayat, M.; Zolfigol, M. A. Green fuel through green route by using a task-specific and neutral 0 CrossMark phosphonium ionic liquid: A joint experimental and theoretical study. *Chem. Eng. J.* **2017,** *309*, 480-488.

(40) Anantharaj, R.; Banerjee, T. Quantum Chemical Studies on the Simultaneous Interaction of Thiophene and Pyridine with Ionic Liquid. *AlChE J.* **2011,** *57*, 749-764.

(41) Cheng, H. Y.; Zhang, J. W.; Qi, Z. W. Effects of interaction with sulphur compounds and free volume in imidazolium-based ionic liquid on desulphurisation: a molecular dynamics study. *Mol. Simul.* **2018,** *44*, 55-62.

(42) Li, H.; Zhang, B.; Jiang, W.; Zhu, W.; Zhang, M.; Wang, C.; Pang, J.; Li, H. A comparative study of the extractive desulfurization mechanism by Cu(II) and Zn-based imidazolium ionic liquids. *Green Energy Environ.* **2019,** *4*, 38-48.

(43) Liu, X. M.; Zhou, G. H.; Zhang, X. P.; Zhang, S. J. Molecular Dynamics Simulation of Desulfurization by Ionic Liquids. *AlChE J.* **2010,** *56*, 2983-2996.

(44) Oliveira, O. V.; Paluch, A. S.; Costa, L. T. A molecular understanding of the phase-behavior of thiophene in the ionic liquid $[C_4mim](+)[BF_4](-)$ for extraction from petroleum streams. *Fuel* **2016,** *175*, 225-231.

(45) Fredenslund, A.; Jones, R. L.; Prausnitz, J. M. Group-contribution estimation of activity coefficients in nonideal liquid mixtures. *AlChE J.* **1975,** *21*, 1086-1099.

(46) Nebig, S.; Gmehling, J. Measurements of different thermodynamic properties of systems

containing ionic liquids and correlation of these properties using modified UNIFAC (Dortmund). *Fluid Phase Equilib.* **2010,** *294*, 206-212.

(47) Lazzus, J. A. A group contribution method to predict the melting point of ionic liquids. *Fluid Phase Equilib*. **2012,** *313*, 1-6.

(48) Lazzus, J. A.; Pulgar-Villarroel, G. A group contribution method to estimate the viscosity of ionic liquids at different temperatures. *J. Mol. Liq.* **2015,** *209*, 161-168.

(49) Paduszynski, K.; Domanska, U. A New Group Contribution Method For Prediction of Density of Pure Ionic Liquids over a Wide Range of Temperature and Pressure. *Ind. Eng. Chem. Res.* **2012,** *51*, 591-604.

(50) Palomar, J.; Ferro, V. R.; Torrecilla, J. S.; Rodriguez, F. Density and molar volume predictions using COSMO-RS for ionic liquids. An approach to solvent design. *Ind. Eng. Chem. Res.* **2007,** *46*, 6041-6048.

(51) Lei, Z.; Dai, C.; Wang, W.; Chen, B. UNIFAC model for ionic liquid-CO_2 systems. *AlChE J.* **2014,** *60*, 716-729.

(52) Karunanithi, A. T.; Mehrkesh, A. Computer-Aided Design of Tailor-Made Ionic Liquids. *AlChE J.* **2013,** *59*, 4627-4640.

(53) Peng, D. L.; Zhang, J. A.; Cheng, H. Y.; Chen, L. F.; Qi, Z. W. Computer-aided ionic liquid design for separation processes based on group contribution method and COSMO-SAC model. *Chem. Eng. Sci.* **2017,** *159*, 58-68.

(54) Mai, N. L.; Koo, Y. M. Computer-Aided Design of Ionic Liquids for High Cellulose Dissolution. *ACS Sustainable Chem. Eng.* **2016,** *4*, 541-547.

(55) Zhao, Y.; Pan, M.; Kang, X.; Tu, W.; Gao, H.; Zhang, X., Gas separation by ionic liquids:

A theoretical study. Chem. Eng. Sci. 2018, 189, 43-55.

(56) Liu, H. J.; Dai, S.; Jiang, D. E. Solubility of Gases in a Common Ionic Liquid from Molecular Dynamics Based Free Energy Calculations. *J. Phys. Chem. B* **2014,** *118*, 2719-2725.

(57) Sprenger, K. G.; Jaeger, V. W.; Pfaendtner, J. The General AMBER Force Field (GAFF) Can Accurately Predict Thermodynamic and Transport Properties of Many Ionic Liquids. *J. Phys. Chem. B* **2015,** *119*, 5882-5895.

(58) Xing, H.; Zhao, X.; Yang, Q.; Su, B.; Bao, Z.; Yang, Y.; Ren, Q. Molecular Dynamics Simulation Study on the Absorption of Ethylene and Acetylene in Ionic Liquids. *Ind. Eng. Chem. Res.* **2013,** *52*, 9308-9316.

Table Captions

Table 1 UNIFAC-IL binary group interaction parameters (a_{nm} and a_{mn}) obtained in this work.

Table 2 Top 5 ILs with the predicted properties in comparison to sulfolane for EDS.

Table 1

Group n	Group m	a_{nm}/K	a_{mn}/K	Group n	Group m	a_{nm}/K	a_{mn}/K
OH	[Cl]	1134.10	-826.58	CH_2=CH	[Cl]	2659.70	2624.50
OH	[BF_4]	-172.83	558.11	CH_2=CH	[BF_4]	541.40	817.25
OH	[PF_6]	-174.12	877.43	CH_2=CH	[PF_6]	906.12	213.90
OH	[FAP]	-251.84	1164.40	CH_2=CH	[FAP]	-299.44	765.01
OH	[NTf_2]	-2.35	282.50	CH_2=CH	[NTf_2]	5.18	99.49
OH	[SCN]	-152.16	-229.50	CH_2=CH	[SCN]	2895.50	2574.50
OH	[$N(CN)_2$]	2390.40	-386.65	CH_2=CH	[$N(CN)_2$]	3230.70	52.33
OH	[$C(CN)_3$]	90.60	-59.69	CH_2=CH	[$C(CN)_3$]	-166.03	2143.30
OH	[$B(CN)_4$]	-111.49	204.96	CH_2=CH	[$B(CN)_4$]	431.21	-163.98
OH	[NO_3]	-282.56	91.10	CH_2=CH	[NO_3]	1358.90	2418.10
OH	[CF_3SO_3]	-30.66	-0.89	CH_2=CH	[CF_3SO_3]	1225.80	-57.03
OH	[CH_3SO_3]	2779.50	-650.99	CH_2=CH	[CH_3SO_3]	2715.40	169.48
OH	[TOS]	-312.99	62.12	CH_2=CH	[TOS]	807.50	74.86
OH	[Im]	-157.75	196.91	CH_2=CH	[Im]	2756.50	471.01
OH	[Py]	-253.59	364.85	CH_2=CH	[Py]	183.44	2472.50
OH	[Pyrro]	-210.31	440.36	CH_2=CH	[Pyrro]	1028.50	147.50
OH	[Pip]	-191.43	498.80	CH_2=CH	[Pip]	3058.70	61.76
OH	[Mmorp]	-107.83	195.21	CH_2=CH	[Mmorp]	912.24	251.23
OH	[iQui]	72.01	-54.47	CH_2CN	[Cl]	-257.72	2068.80
OH	[N]	2584.40	425.10	CH_2CN	[BF_4]	-171.44	2236.10
OCH_3	[Cl]	2572.40	2465.10	CH_2CN	[FAP]	2135.30	-372.61
OCH_3	[BF_4]	292.16	280.51	CH_2CN	[NTf_2]	205.44	-176.26
OCH_3	[FAP]	3886.20	-534.02	CH_2CN	[SCN]	730.58	-195.74
OCH_3	[NTf_2]	2831.60	-287.29	CH_2CN	[$N(CN)_2$]	-118.61	2851.70
OCH_3	[SCN]	976.06	3066.70	CH_2CN	[$C(CN)_3$]	46.16	-67.03
OCH_3	[$N(CN)_2$]	3615.40	-22.83	CH_2CN	[$B(CN)_4$]	257.48	-281.51
OCH_3	[$C(CN)_3$]	-273.82	457.34	CH_2CN	[NO_3]	-218.38	1149.90
OCH_3	[$B(CN)_4$]	-229.98	249.07	CH_2CN	[CF_3SO_3]	20.08	90.22
OCH_3	[NO_3]	2050.90	-220.00	CH_2CN	[CH_3SO_3]	2507.50	-135.56
OCH_3	[CF_3SO_3]	-223.69	576.25	CH_2CN	[Im]	234.36	-1.73
OCH_3	[CH_3SO_3]	2964.90	26.54	CH_2CN	[Py]	240.15	-84.27
OCH_3	[TOS]	107.18	472.00	CH_2CN	[Pyrro]	747.66	-147.21
OCH_3	[Im]	3299.80	-62.30	CH_2CN	[Pip]	587.13	-85.93
OCH_3	[Py]	-61.95	271.96	CH_2CN	[Mmorp]	-92.11	1127.00
OCH_3	[Pyrro]	-188.30	1131.30	CH_2CN	[iQui]	-57.74	486.19
OCH_3	[Pip]	-51.74	594.48	CH_3CN	[N]	2624.80	-37.73
OCH_3	[Mmorp]	-140.70	3230.30	CH_2CN	[Cl]	-257.72	2068.80
OCH_3	[iQui]	123.27	353.03	CH_2CN	[BF_4]	-171.44	2236.10
OCH_3	[N]	2867.70	2459.70				

Table 2

No.	Group Combination	β	S	PI	T_m (K)	η (cP)
1	$1CH_2$=CH, $1CH_2$, 1[MPy], 1[$C(CN)_3$]	1.98	17.78	35.24	276.6	21.6
2	$1CH_2$=CH, $1CH_2$, 1[Py], 1[$C(CN)_3$]	1.94	15.55	30.17	260.0	15.6
3	$1CH_2$=CH, $2CH_2$, 1[MPy], 1[$C(CN)_3$]	1.84	16.40	30.15	272.8	25.2
4	$1CH_2$=CH, $3CH_2$, 1[MPy], 1[$C(CN)_3$]	1.74	15.22	26.52	269.1	29.5
5	$1CH_2$=CH, $2CH_2$, 1[Py], 1[$C(CN)_3$]	1.79	14.10	25.21	256.2	18.2
Ref.	sulfolane	0.79	11.13	8.75	300.7	10.1

Figure Captions

Figure 1 (a) Comparison of experimental and UNIFAC-IL calculated γ^{∞} for different solutes in ILs and (b) distribution of data points within different ranges of absolute relative deviations.

Figure 2 Comparison of experimental and UNIFAC-IL calculated LLE data for (a) {[OHC_3Py][$N(CN)_2$] + cyclohexene + cyclohexane}, (b){[COC_2mPip][NTf_2] + *n*-heptane + methanol}, (c) {[CH_2=CHC_1Mor][NTf_2] + benzene + *n*-hexane}, and (d) {[C_3CNPy][$N(CN)_2$] + styrene + ethylbenzene}.

Figure 3 Structures of the top five functional ILs identified by CAILD.

Figure 4 Comparison of (a) β, (b) *S*, and (c) *PI* of the designed top five functional ILs (F1 – F5) with the previously reported conventional ILs (C1 – C5).

Figure 5 Optimized structures of $[CH_2=CHC1MPy]^+$, $[C_2MPy]^+$, $[C(CN)_3]^-$, thiophene, *n*-octane, toluene and cyclohexane together with their atom labels.

Figure 6 SDFs of anion (red), cation skeleton (orange) and substituents (ice blue) around thiophene in (a) {[CH_2=CHC_1MPy][$C(CN)_3$] + model fuel oil} and (b) {[C_2MPy][$C(CN)_3$] + model fuel oil} systems (isovalues of the red, orange and ice blue regions corresponding to 0.25, 0.25, 0.4 Å, respectively).

Figure 7 RDFs of substituents – thiophene in {[CH_2=CHC_1MPy][$C(CN)_3$] +model fuel oil} (solid line) and {[C_2MPy][$C(CN)_3$] + model fuel oil} (dash line) systems.

Figure 8 RDFs of (a) substituents – *n*-octane, (b) substituents – toluene and (c) substituents – cyclohexane in {[CH_2=CHC_1MPy][$C(CN)_3$] + model fuel oil} (solid line) and {[C_2MPy][$C(CN)_3$] + model fuel oil} (dash line) systems.

Figure 1

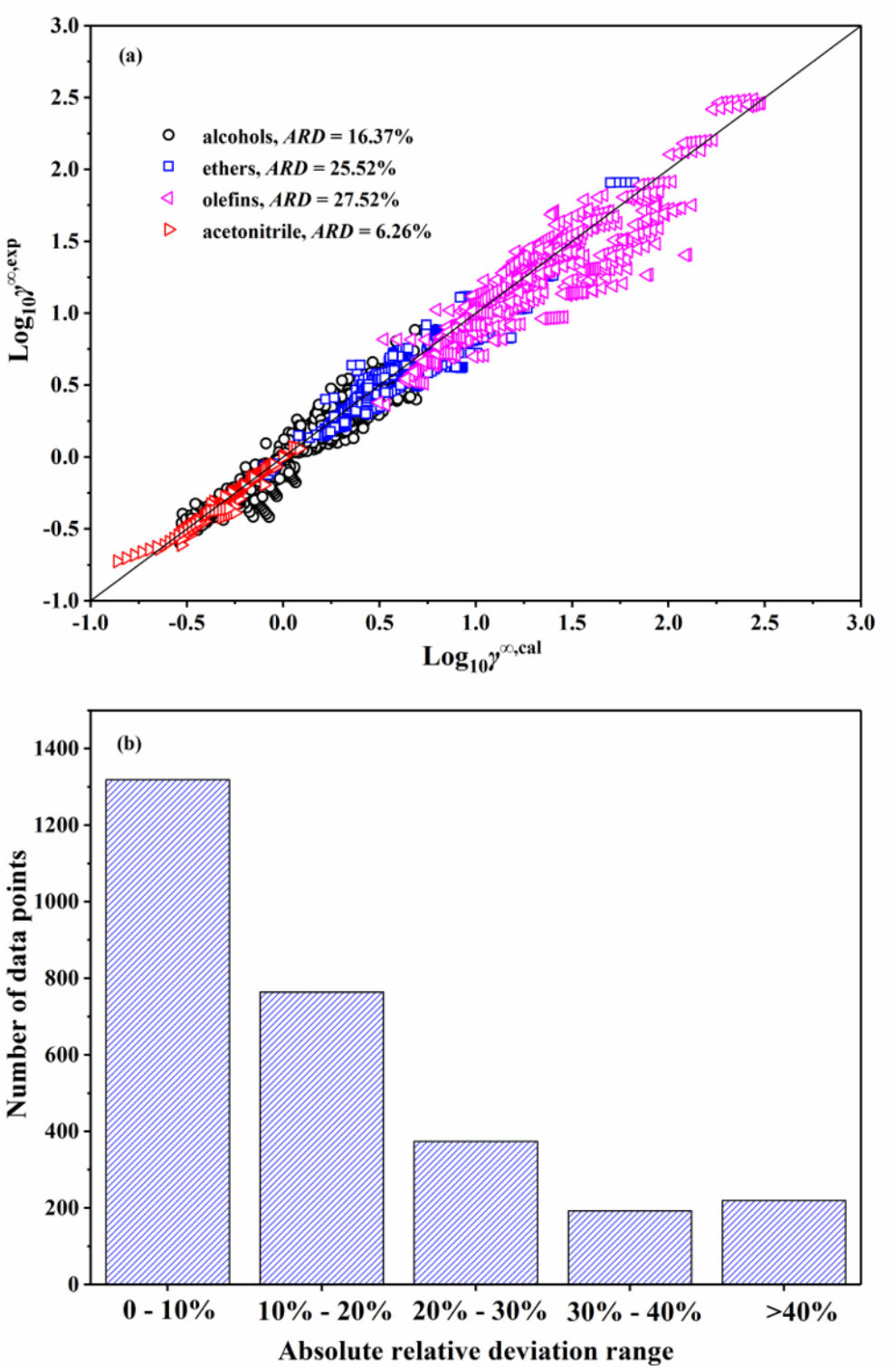
(a)
alcohols, ARD = 16.37%
ethers, ARD = 25.52%
olefins, ARD = 27.52%
acetonitrile, ARD = 6.26%
Log10γ∞,exp
Log10γ∞,cal
3.0
2.5
2.0
1.5
1.0
0.5
0.0
-0.5
-1.0
(b)
Number of data points
1400
1200
1000
800
600
400
200
0
0 - 10%
10% - 20%
20% - 30%
30% - 40%
>40%
Absolute relative deviation range

Figure 2

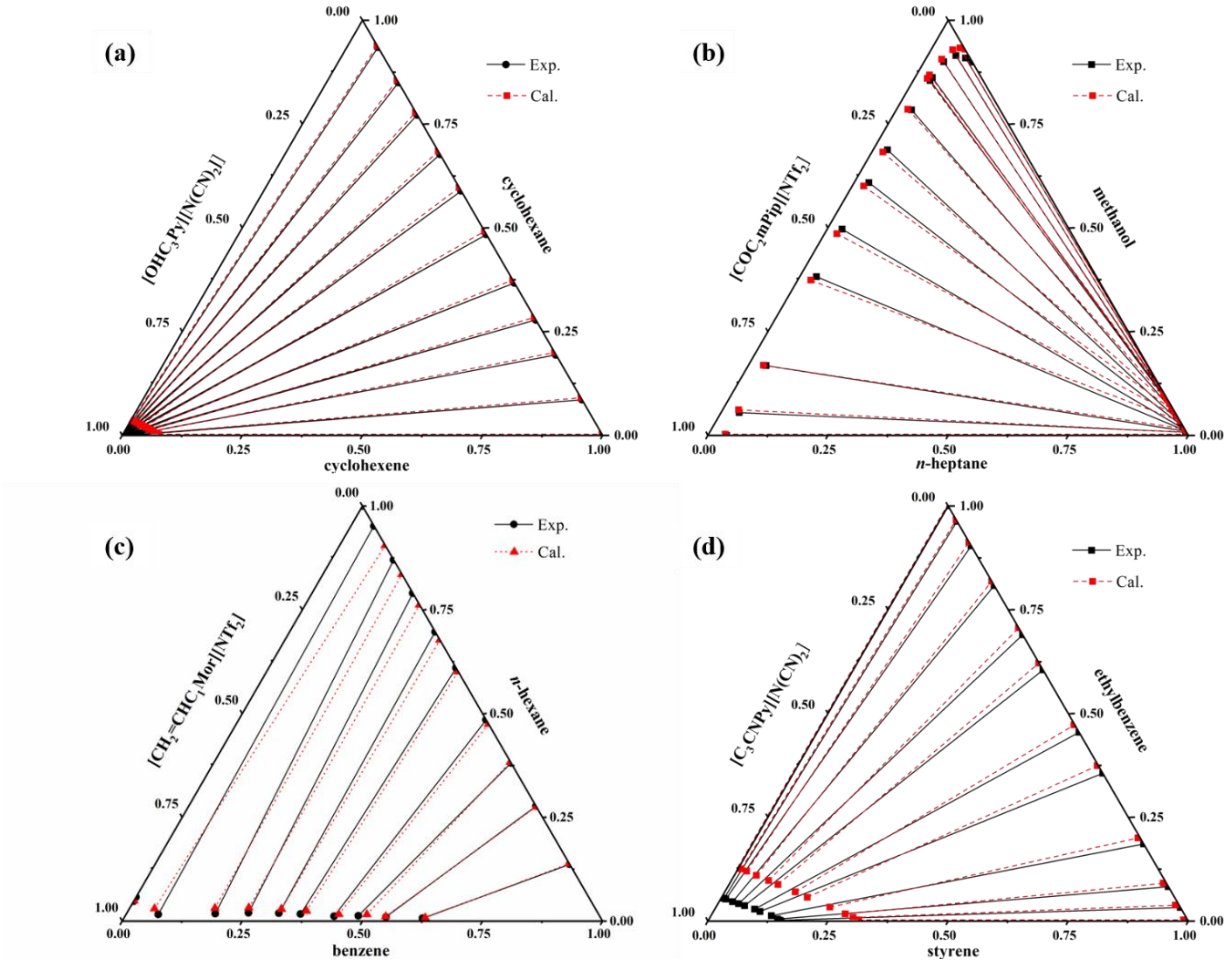
(a)
Exp.
Cal.
[OHC2Py][N(CN)2]
cyclohexane
cyclohexene
(b)
Exp.
Cal.
[COC2piPip][NTf2]
methanol
n-heptane
(c)
Exp.
Cal.
[CH2=CHC1Mor][NTf2]
n-hexane
benzene
(d)
Exp.
Cal.
[C3CNPy][N(CN)2]
ethylbenzene
styrene

Figure 3

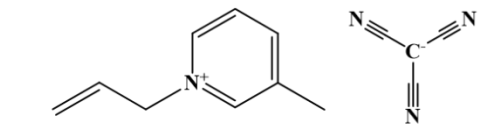

IL1

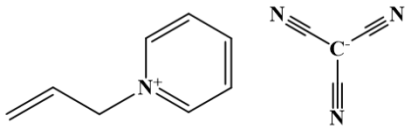

IL2

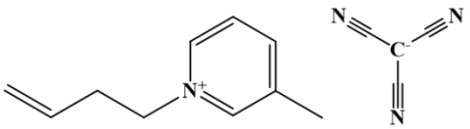

IL3

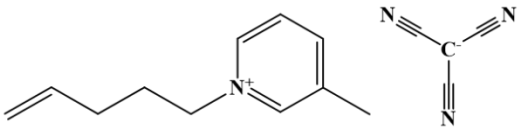

IL4

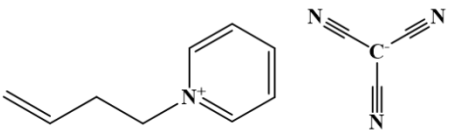

IL5

Figure 4

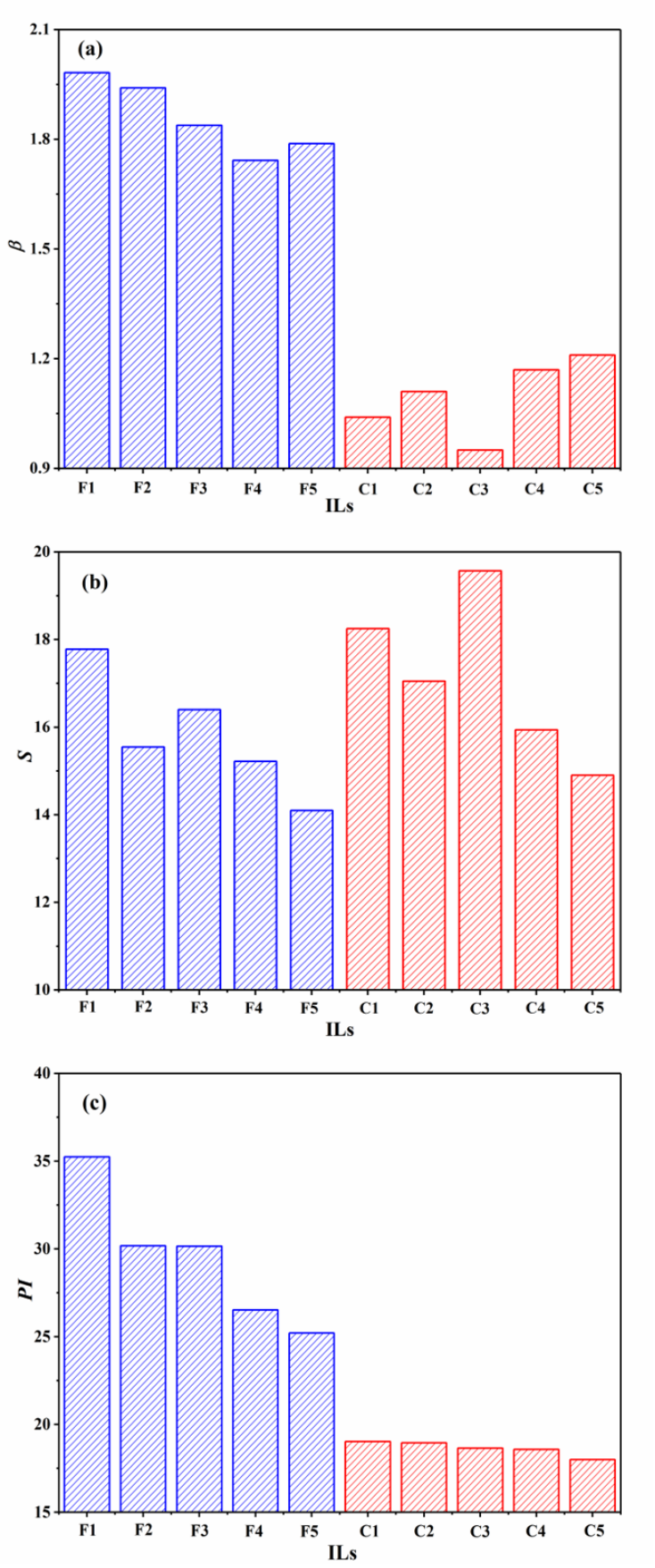
(a)
β
2.1
1.8
1.5
1.2
0.9
F1 F2 F3 F4 F5 C1 C2 C3 C4 C5
ILs
(b)
S
20
18
16
14
12
10
F1 F2 F3 F4 F5 C1 C2 C3 C4 C5
ILs
(c)
PI
40
35
30
25
20
15
F1 F2 F3 F4 F5 C1 C2 C3 C4 C5
ILs

Figure 5

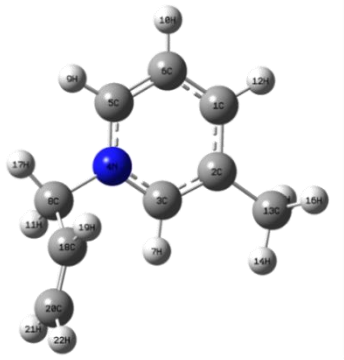

$[CH_2{=}CHC_1MPy]^+$

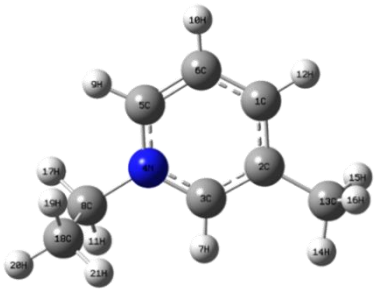

$[C_2MPy]^+$

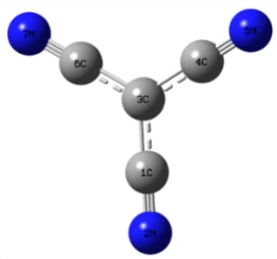

$[C(CN)_3]^-$

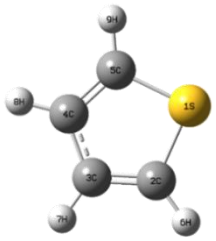

thiophene

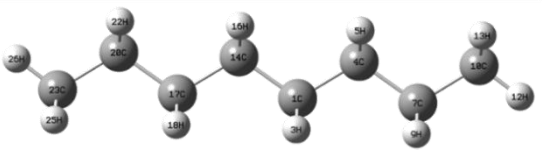

n-octane

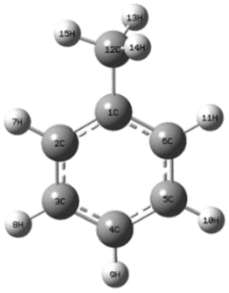

toluene

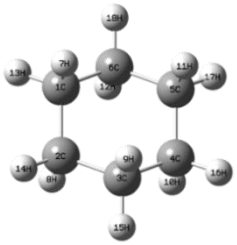

cyclohexane

Figure 6

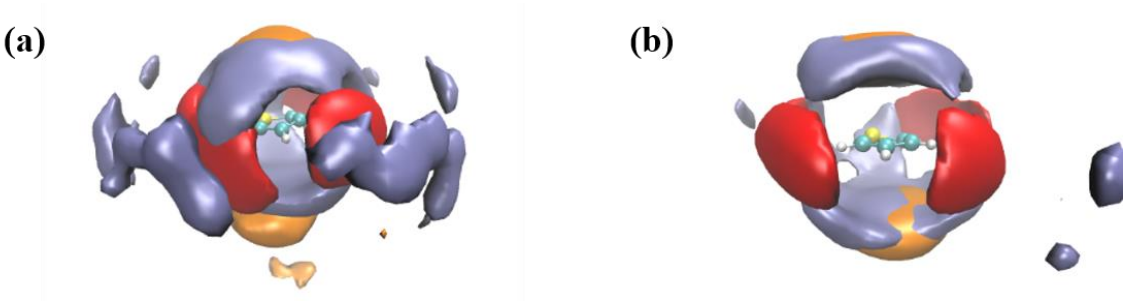

Figure 7

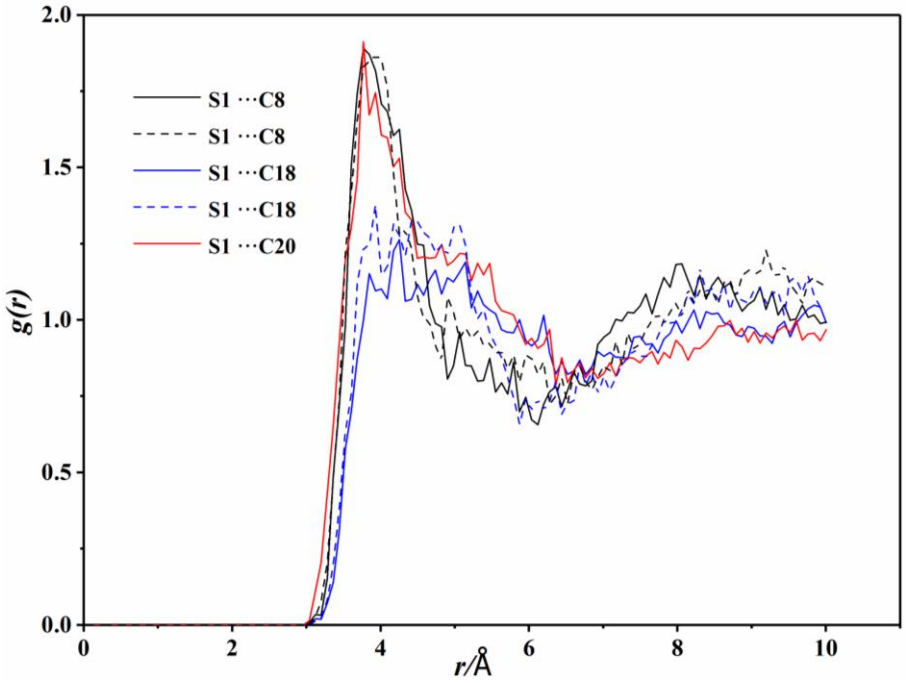

Figure 8

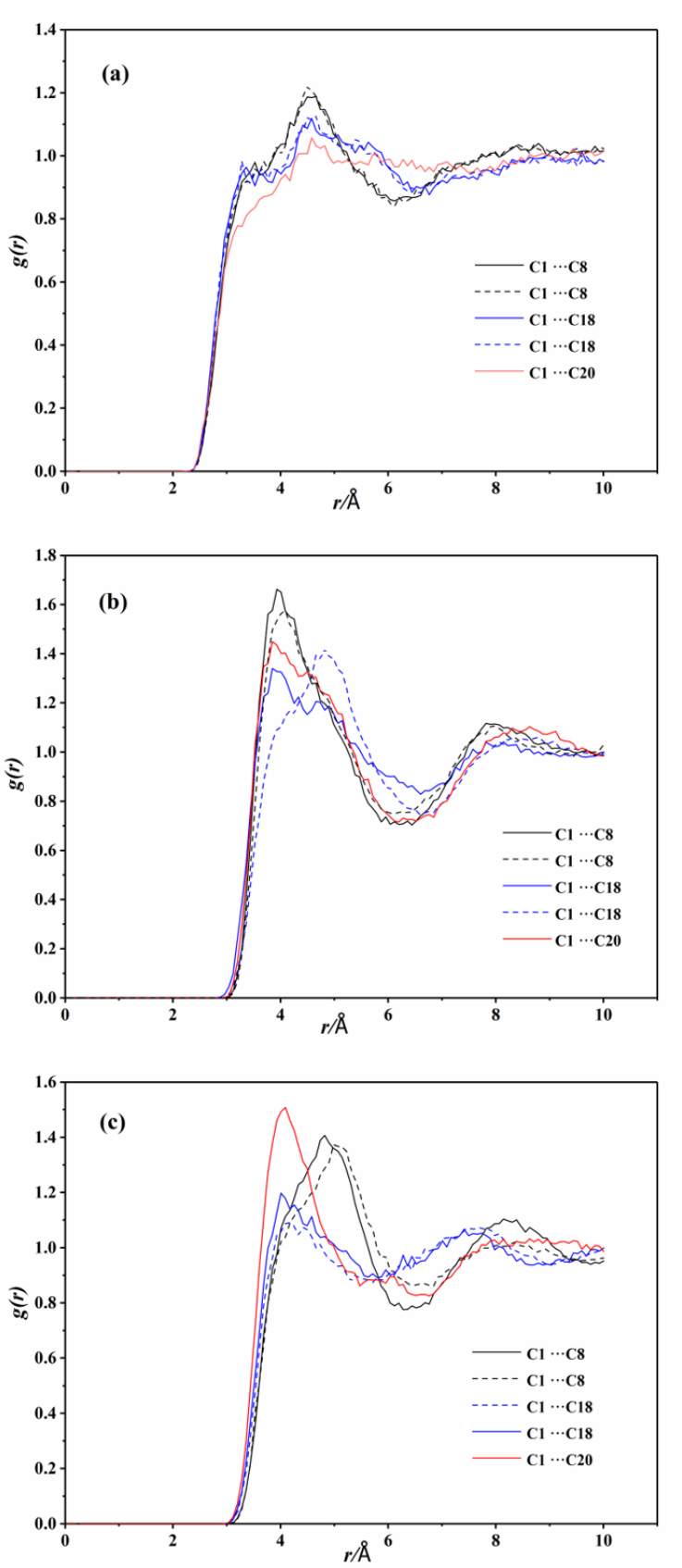
(a)
g(r)
r/Å
C1 ···C8
C1 ···C8
C1 ···C18
C1 ···C18
C1 ···C20
(b)
g(r)
r/Å
C1 ···C8
C1 ···C8
C1 ···C18
C1 ···C18
C1 ···C20
(c)
g(r)
r/Å
C1 ···C8
C1 ···C8
C1 ···C18
C1 ···C18
C1 ···C20

Table of Contents

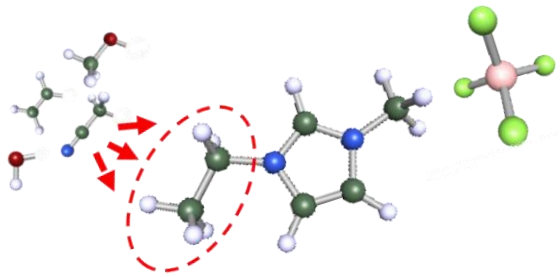

IL functionalization

Structure design

Microscopic insights

CAILD

Promising candidates

MD simulations

OF: $\max\{PI = \beta \times S\}$

s.t. Structural constraints

Thermodynamic property constraints

Physical property constraints